Neurochemistry International 61 (2012) 749–758

Contents lists available at SciVerse ScienceDirect

Neurochemistry International

journal homepage: www.elsevier.com/locate/nci

Differential participation of phospholipase A_2 isoforms during iron-induced retinal toxicity. Implications for age-related macular degeneration

G. Rodríguez Diez, R.M. Uranga [1], M.V. Mateos [1], N.M. Giusto, G.A. Salvador *

Instituto de Investigaciones Bioquímicas de Bahía Blanca, Universidad Nacional del Sur and Consejo Nacional de Investigaciones Científicas y Técnicas, 8000 Bahía Blanca, Argentina

ARTICLE INFO

Article history:
Received 13 December 2011
Received in revised form 6 June 2012
Accepted 14 June 2012
Available online 22 June 2012 22 June 2012

In memoriam Dr. Paula I. Castagnet

Keywords:
Retina
Iron
PLA_2
Oxidative stress
AMD
COX-2

ABSTRACT

Both elevated iron concentrations and the resulting oxidative stress condition are common signs in retinas of patients with age-related macular degeneration (AMD). The role of phospholipase A_2 (PLA_2) during iron-induced retinal toxicity was investigated. To this end, isolated retinas were exposed to increasing Fe^{2+} concentrations (25, 200 or 800 μM) or to the vehicle, and lipid peroxidation levels, mitochondrial function, and the activities of cytosolic PLA_2 ($cPLA_2$) and calcium-independent PLA_2 ($iPLA_2$) were studied. Incubation with Fe^{2+} led to a time- and concentration-dependent increase in retinal lipid peroxidation levels whereas retinal cell viability was only affected after 60 min of oxidative injury.

A differential release of arachidonic acid (AA) and palmitic acid (PAL) catalyzed by $cPLA_2$ and $iPLA_2$ activities, respectively, was also observed in microsomal and cytosolic fractions obtained from retinas incubated with iron. AA release diminished as the association of cyclooxigenase-2 increased in microsomes from retinas exposed to iron. Retinal lipid peroxidation and cell viability were also analyzed in the presence of $cPLA_2$ inhibitor, arachidonoyl trifluoromethyl ketone (ATK), and in the presence of $iPLA_2$ inhibitor, bromoenol lactone (BEL). ATK decreased lipid peroxidation levels and also ERK1/2 activation without affecting cell viability. BEL showed the opposite effect on lipid peroxidation. Our results demonstrate that $iPLA_2$ and $cPLA_2$ are differentially regulated and that they selectively participate in retinal signaling in an experimental model resembling AMD.

1. Introduction

Metallo-neurobiology has undergone a significant evolution in the last 20 years. Still, although there is much experimental evidence on various aspects of the involvement of iron in several neurodegenerative diseases, the role of this metal in the central nervous system and, particularly, in neurodegenerative processes has not been fully elucidated to date (Dunaief, 2006).

Iron is necessary for normal retinal cellular function. Still, iron overload has been found to be associated with retinal degenerative disorders such as ocular siderosis, intraocular hemorrhage, and the hereditary diseases aceruloplasminemia and pantothenate kinase-associated neurodegeneration (Dunaief et al., 2005; Dunaief, 2006; Hadziahmetovic et al., 2008; Hahn et al., 2004; He et al., 2007; Wong et al., 2007). Furthermore, it is well known that reactive oxygen species (ROS) may contribute to the pathogenesis of age-related macular degeneration (AMD) and that they can be produced in the Fenton reaction catalyzed by ferric (Fe^{3+}) and ferrous (Fe^{2+}) ions (Lukinova et al., 2009). Previous post mortem research has found that iron concentrations are higher in AMD retinas than in non-affected retinas (Blasiak et al., 2011). In addition, the age-related increase of iron levels in the macula, the up-regulation of transferrin in AMD, the development of AMD-like

Abbreviations: [^{14}C]DPPC, 1-[^{14}C]palmitoyl-2-[^{14}C]palmitoyl-sn-glycero-3-phosphocholine; [^{14}C]PAPC, 1-palmitoyl-2-[^{14}C]arachidonoyl-sn-glycero-3-phosphocholine; 4-HNE, 4-hydroxynonenal; AA, arachidonic acid; AMD, age-related macular degeneration; ATK, arachidonoyl trifluoromethyl ketone; ATP, adenosine-5′-triphosphate; BEL, bromoenol lactone; BSA, bovine serum albumin; COX, cyclooxigenase; $cPLA_2$, cytosolic phospholipase A_2; DTT, dithiothreitol; EDTA, *N*,*N*′-1,2-ethandiylbis[*N*-(carboxymethyl)glycine] disodium salt; ERK1/2, extracellular signal-regulated kinases; HEPES, 4-(2-hydroxyethyl)-1-piperazine ethanesulfonic acid; HRP, horseradish peroxidase; $iPLA_2$, calcium-independent phospholipase A_2; MAPK, mitogen-activated protein kinases; MEK, mitogen-activated protein kinase kinase; MTT, 3-(4,5-dimethylthiazol-2-yl)-2,5-diphenyltetrazolium bromide; NBIA, neuronal brain iron accumulation; PAL, palmitic acid; PBS, phosphate buffer saline; PLA_2, phospholipase A_2; PMSF, phenylmethylsulfonyl fluoride; RD, retinal degeneration; ROS, reactive oxygen species; SDS, sodium dodecyl sulfate; SDS–PAGE, sodium dodecyl sulfate–polyacrylamide gel electrophoresis; TBA, thiobarbituric acid; TBARS, thiobarbituric acid reactive substances; U0126, 1,4-diamino-2,3-dicyano-1,4-bis[2-aminophenylthio]butadiene.

* Corresponding author. Address: Instituto de Investigaciones Bioquímicas de Bahía Blanca, Centro Científico y Tecnológico CONICET Bahía Blanca and Universidad Nacional del Sur, Edificio E1, Camino La Carrindanga km 7, 8000 Bahía Blanca, Argentina. Tel.: +54 291 4861201; fax: +54 291 4861200.

E-mail address: salvador@criba.edu.ar (G.A. Salvador).

[1] These authors contributed equally to this work.

0197-0186/$ - see front matter © 2012 Elsevier Ltd. All rights reserved.
http://dx.doi.org/10.1016/j.neuint.2012.06.012

syndromes in ceruloplasmin- and hephaestin-deficient mice, and the association between polymorphism of iron homeostasis genes and AMD support the leading role of this metal in this pathology (Blasiak et al., 2011; Garcia-Castineiras, 2010; Hadziahmetovic et al., 2008; Wong et al., 2007). Another disease also characterized by excessive iron accumulation is hemochromatosis. Most patients with hereditary hemochromatosis have a mutation in the histocompatibility leukocyte antigen class I-like protein involved in iron homeostasis (HFE) gene product (Feder et al., 1996). This protein forms, in general, a stable complex with the transferrin receptor, lowering its affinity for transferrin (Feder et al., 1998). Patients with mutations in the HFE gene evidence elevated transferrin binding to transferrin receptors, ending in, in turn, a higher iron uptake into tissues. This genetic disorder is also associated with retinal abnormalities, including, in some cases, retinal pigment epithelium atrophy or angioid streaks. Furthermore, a study conducted in two postmortem patients also showed drusen formation, the clinical hallmark of AMD (Dunaief, 2006).

On the other hand, several neurodegenerative disorders with neuronal brain iron accumulation (NBIA) have been associated with defective phospholipase A_2 (PLA_2) signaling. Mutations in PLA2G6 gene, which encodes a calcium-independent group VI PLA_2, have been reported in NBIA (Morgan et al., 2006). Moreover, the up-regulation of secretory phospholipase A_2 IIA and its participation in neuronal apoptosis have been reported during cerebral ischemia (Adibhatla and Hatcher, 2010; Yagami et al., 2002). PLA_2s belong to a superfamily of enzymes that hydrolyze the sn-2 fatty acids of membrane phospholipids. These proteins are known to play multiple roles related to the maintenance of membrane phospholipid homeostasis and production of a variety of lipid mediators (Burke and Dennis, 2009b). There are more than 20 different types of PLA_2s and, in spite of their common function in hydrolyzing phospholipid fatty acids, they are diversely encoded by a number of genes and are regulated by different mechanisms. The most recent classification involves the following main groups: (i) low molecular secretory PLA_2 ($sPLA_2$) which includes groups I–III, V and IX–XIV; (ii) high molecular calcium-dependent cytosolic PLA_2 ($cPLA_2$) which includes groups IVA–IVF; (iii) high molecular calcium-independent PLA_2 ($iPLA_2$) which includes groups VIA-1, VIA-2 and VIB–VIF; and (iv) platelet-activating factor acetylhydrolase which includes groups VIIA–VIIB and VIIIA–VIIIB (Burke and Dennis, 2009a; Sun et al., 2010).

Although the physiological role of these PLA_2s in the regulation of neuronal cell function has not yet been fully elucidated, there is increasing evidence about their involvement in receptor signaling and transcriptional pathways that link oxidative events to inflammatory responses underlying many neurodegenerative diseases (Sun et al., 2007). Previous research also revealed the important role of $cPLA_2$, $sPLA_2$ and $iPLA_2$ in modulating neuronal excitatory functions, in the inflammatory responses, and, as stated above, in childhood neurological disorders associated with NBIA, respectively (Farooqui et al., 2006; Morgan et al., 2006; Moses et al., 2006; Svensson et al., 2005). Furthermore, the up-regulation of mRNA of various subgroups of $sPLA_2$ during light-induced retinal degeneration (RD) has been reported particularly in the retina (Tanito et al., 2008; Yang et al., 2008). Moreover, the increase in arachidonic acid (AA) release, one of the main products of PLA_2 action, has been suggested to be involved in the pathogenesis of RD (Kashiwagi et al., 2000; Wang and Kolko, 2010). $iPLA_2$ expression has also been involved in the proliferation of retinal pigment epithelium cells during RD associated with AMD (Kolko et al., 2009). Evidence presented here shows a correlation between iron, RD and PLA_2-derived signaling. However, the specific role of PLA_2s in RD still remains unknown. Thus, taking into account this background, the main goal of the present work was to characterize PLA_2 activities and their regulation in an experimental model of RD. To this end, isolated bovine retinas were exposed to increasing Fe^{2+} concentrations, and cellular viability, lipid peroxidation levels and $cPLA_2$ and $iPLA_2$ activities were analyzed. The role of PLA_2 isoforms in retinal damage and the involvement of mitogen-activated protein kinase (MAPK) ERK1/2 in PLA_2 regulation were also studied.

2. Materials and methods

2.1. Materials

1-Palmitoyl-2-[^{14}C]arachidonoyl-sn-glycero-3-phosphocholine (38.0 mCi/mmol, [^{14}C]PAPC) and 1-[^{14}C]palmitoyl-2-[^{14}C]palmitoyl-sn-glycero-3-phosphocholine (111.0 mCi/mmol, [^{14}C]DPPC) were obtained from New England Nuclear-Dupont (Boston, MA, USA). PLA_2 inhibitors [arachidonoyl trifluoromethyl ketone (ATK) and bromoenol lactone (BEL)], mitogen-activated protein kinase kinase (MEK) 1/2 inhibitor [1,4-diamino-2,3-dicyano-1,4-bis[2-aminophenylthio]butadiene (U0126)], Triton X-100, 3-[4,5-dimethylthiazol-2-yl]-2,5-diphenyltetrazolium bromide (MTT), and thiobarbituric acid (TBA) were obtained from Sigma–Aldrich (St. Louis, MO, USA). All other chemicals were of the highest purity available. Mouse polyclonal IgG2a, anti-phospho-Tyr204-extracellular signal-regulated kinases (ERK) 1/2, rabbit polyclonal anti-phosphotyrosine (PY20), rabbit polyclonal anti-ERK2, rabbit polyclonal anti-phospho-Thr180/Tyr182-p38, rabbit polyclonal anti-β-tubulin, rabbit polyclonal anti-calnexin, polyclonal horseradish peroxidase (HRP)-conjugated goat anti-rabbit IgG, and polyclonal HRP-conjugated goat anti-mouse IgG were purchased from Santa Cruz Biotechnology, Inc. (Santa Cruz, CA, USA). Rabbit polyclonal anti-cyclooxygenase (COX)-2 was purchased from Cayman Chemical (Ann Arbor, MI, USA). Rabbit anti-phospho-Ser505-$cPLA_2$ was purchased from Cell Signaling Technology (Boston, MA, USA).

2.2. Experimental treatments

Fresh bovine eyes were obtained from a local abattoir and placed and stored in crushed ice. Retinas were dissected on ice (4 °C) under normal lighting conditions and washed with saline solution. Entire retinas were preincubated at 37 °C for 30 min with either inhibitors (50 μM ATK, 25 μM BEL or 10 μM U0126) or the vehicle, and they were subsequently exposed for 5 or 60 min to either $FeSO_4$ (25, 200 or 800 μM) or its vehicle as previously described (Uranga et al., 2007). Entire retinas were incubated under an O_2:CO_2 (95:5, vol/vol) atmosphere with gentle agitation for all experiments. All incubations were performed in Locke's buffer [154 mM NaCl, 5.6 mM KCl, 3.6 mM $NaHCO_3$, 1 mM $MgCl_2$, 2.3 mM $CaCl_2$, 5 mg/ml glucose, 5 mM 4-(2-hydroxyethyl)-1-piperazine ethanesulfonic acid (HEPES), pH 7.2] unless stated otherwise. After incubation, retinas were washed in Locke's buffer to be further used for experimental procedures.

2.3. Isolation of subcellular fractions

Subcellular fractions were obtained as previously described with slight modifications (Salvador and Giusto, 2006). Briefly, homogenates (20% wt/vol) from the dissected retinas to be used for subcellular fractionation were prepared in a medium containing 0.32 M sucrose, 1 mM *N*,*N*′-1,2-ethandiylbis[*N*-(carboxymethyl)glycine] disodium salt (EDTA), 1 mM dithiothreitol (DTT), 2 mg/ml leupeptin, 1 mg/ml aprotinin, 1 mg/ml pepstatin, 0.1 mM phenylmethylsulfonyl fluoride (PMSF), and 10 mM HEPES (pH 7.4). Homogenates to be used for MTT reduction, thiobarbituric acid reactive substances (TBARS) and Western blot assays, and

radical scavenging measurement were prepared in Locke's buffer. Independently of the buffer used, retinas were homogenized by 10 strokes with a Thomas tissue homogenizer. Homogenates were centrifuged at 1800×*g* for 7.5 min at 4 °C using a JA-21 rotor in a Beckman J2-21 centrifuge. The pellet (corresponding to crude nuclear fraction and cellular debris) was discarded and the supernatant was retained and centrifuged at 14,000×*g* for 20 min at 4 °C. The mitochondrial pellet was stored at −80 °C, and the supernatant was centrifuged at 85,500×*g* for 1 h at 4 °C using a SW28.1 rotor in a Beckman Optima LK-90 ultracentrifuge. The final pellet was considered as microsomal fraction and the supernatant as cytosolic fraction. Total homogenates and microsomal and cytosolic fractions were used for the experiments detailed below. Protein content of retinal subcellular fractions was determined following Lowry (Lowry et al., 1951).

2.4. PLA_2 activity assays

To determine $cPLA_2$ activity, sn-2 fatty acid hydrolysis was determined using lipid vesicles containing [^{14}C]PAPC and cold 1-palmitoyl-2-oleoyl-sn-glycero-3-phosphocholine to yield 60,000 dpm (0.100 mM) per assay in a buffer containing 0.025% Triton X-100, 0.16 mM $CaCl_2$, 0.2 mg/ml bovine serum albumin (BSA), 4 mM DTT, 100 mM HEPES, pH 7.5 (Svensson et al., 2005). In order to analyze the involvement of phospholipase A_1/lysophospholipase A_2 activity in AA generation, lysophospholipid formation from [^{14}C]PAPC was measured under the same experimental conditions as those used for $cPLA_2$ activity. These assays were performed either in the presence or in the absence of 2 mM PMSF (as lysophospholipase A_2 inhibitor) (Pete et al., 1996).

To determine $iPLA_2$ activity, sn-2 fatty acid hydrolysis was determined using lipid vesicles containing [^{14}C]DPPC and cold DPPC to yield 60,000 dpm (0.100 mM) per assay in a buffer containing 0.025% Triton X-100, 10 mM EDTA, 2 mM adenosine-5′-triphosphate (ATP), 100 mM HEPES, pH 7.5 (Svensson et al., 2005). Seventy-five microlitres of the corresponding lipid vesicles were added to 75 μl of treated retinal subcellular fractions (150 μg of protein, final volume 150 μl).

All reactions were carried out at 37 °C for 20 min, with gentle agitation, and stopped by the addition of 5 ml of chloroform/methanol (2:1, vol/vol).

2.5. Extraction and isolation of lipids

Lipids were extracted according to Folch et al. (1957) the lipid extract was subsequently washed with 0.2 volumes of 0.05% $CaCl_2$ and the lowest phase was obtained after centrifugation at 900×*g* for 5 min. Neutral lipids monoacylglycerol, diacylglycerol, and free fatty acids were then separated by one-dimensional thin-layer chromatography using silica gel G plates (Merck) in a mobile phase consisting of hexane/diethyl ether/acetic acid (50:50:2.6, vol/vol). DPPC and PAPC as well as the remaining retinal phospholipids were retained at the spotting site. Lipids were visualized by exposure of the plate to iodine vapors. The spots corresponding to free fatty acids were scraped off the plate and quantified by liquid scintillation.

Lysophospholipids were separated from phospholipids and neutral lipids by one-dimensional thin-layer chromatography using silica gel H plates (Merck) in a mobile phase consisting of chloroform/methanol/ammonia (65:25:5, vol/vol). Lipids were visualized by exposure of the plate to iodine vapors. The spots corresponding to lysophospholipids and phospholipids were scraped off the plate and quantified by liquid scintillation.

2.6. MTT reduction assay

To determine retinal reducing activity, the extent of MTT reduction to insoluble intracellular formazan crystals was measured. This reduction depends on the activity of intracellular dehydrogenases and is independent of the changes in the plasma membrane integrity. MTT reduction was measured in total homogenates obtained from entire retinas exposed to either 25, 200 and 800 μM $FeSO_4$ or to the vehicle, and in the presence or absence of the corresponding inhibitors. The method used in the present study has been previously described (Uranga et al., 2007). Briefly, MTT was dissolved in phosphate buffer saline (PBS) at a concentration of 5 mg/ml. MTT solution was mixed with total homogenate (1:10; MTT:homogenate, vol/vol) and allowed to incubate for 2 h at 37 °C with gentle agitation. At the end of incubation with MTT, 300 μl of solubilization buffer [20% sodium dodecyl sulfate (SDS), pH 4.7] were added and mixed thoroughly to dissolve formazan crystals. The extent of MTT reduction was then measured spectrophotometrically at 570 nm with the absorbance at 650 nm subtracted to account for cellular debris. Results were expressed as final optical density values.

2.7. COX-2 activity assays

To determine COX-2 activity, the generation of prostaglandins F and E (PGF_2 and PGE_2) was measured by using lipid vesicles containing [^{14}C]arachidonic acid to yield 60,000 dpm (0.100 mM) per assay in a buffer containing 0.025% Triton X-100, 0.16 mM $CaCl_2$, 0.2 mg/ml BSA, 4 mM DTT, 100 mM HEPES, pH 7.5. Reactions were carried out at 37 °C for 20 min, with gentle agitation, and stopped by the addition of 5 ml of chloroform/methanol (2:1, vol/vol). Prostaglandins were then separated as described by Franchi et al. (2000), by one-dimensional thin-layer chromatography using silica gel G plates (Merck) in a mobile phase consisting of bencene/dioxane/acetic acid (60:30:3, vol/vol) and purified standards of PGE_2 and PGF_2. PGE_2 and PGF_2 were visualized by exposure of the plate to iodine vapors. The corresponding spots were scraped off the plate and quantified by liquid scintillation.

2.8. Lipid peroxidation assay

Lipid peroxidation was measured using the TBA assay as previously described (Mateos et al., 2008). Briefly, after incubation in the presence of either Fe^{2+} or the vehicle, and in the presence or absence of the corresponding inhibitors, 1 ml of 30% TCA was added to 0.5 ml of total homogenate (1.5 mg protein/ml). Then, 0.1 ml of 5 N HCl and 1 ml of 0.75% TBA were added. Tubes were capped, the mixtures were heated at 100 °C for 15 min in a boiling water bath and samples were centrifuged at 1000×*g* for 10 min. TBARS were measured in the supernatant at 535 nm. Results were expressed as units of absorbance at 535 nm per mg of protein [Abs 535 nm (arbitrary units)/mg protein].

2.9. SDS–PAGE and Western blot assays

Samples from total homogenates and microsomal and cytosolic fractions were denatured with Laemmli sample buffer at 100 °C for 5 min (Laemmli, 1970). Equivalent amounts of proteins were separated by SDS–polyacrylamide gel electrophoresis (SDS–PAGE) on 10% polyacrylamide gels and then transferred to a polyvinylidene fluoride membrane (Millipore, Bedford, MA) using a Mini Trans-Blot cell electroblotter (BIO-RAD Life Science Group, California) for 2 h. Membranes were blocked with 5% nonfat dry milk in TTBS buffer [20 mM Tris–HCl, pH 7.5, 100 mM NaCl, and 0.1% (wt/vol) Tween 20] for 1 h at room temperature. Membranes were then incubated with the following primary antibodies: (i) anti-COX-2

(1:1000) or anti-phospho-p38 (1:1000) overnight at 4 °C, or (ii) anti-phospho-ERK1/2 (1:1000), anti-β-tubulin (1:1000), anti-ERK2 (1:2000) and anti-phosphotyrosine PY20 (1:750) for 2 h at room temperature. After incubation membranes were, washed three times with TTBS, and then exposed to the appropriate HRP-conjugated secondary antibody (anti-rabbit or anti-mouse) for 1 h at room temperature. Membranes were again washed three times with TTBS. Immunoreactive bands were detected by enhanced chemiluminescence (ECL; Amersham Biosciences, USA) using standard X-ray film (ECL, Amersham Biosciences, USA). Immunoreactive bands were quantified using image analysis software (Image J, a freely available application in the public domain for image analysis and processing, developed and maintained by Wayne Rasband at the Research Services Branch, National Institute of Mental Health).

2.10. Statistical analysis

Statistical analysis was performed using one-way ANOVA test to compare means and followed by Fisher's least significant difference (LSD) test. *p*-Values lower than 0.05 were considered statistically significant.

3. Results

3.1. Determination of cellular damage during iron-induced retinal toxicity

Our first goal was the characterization of iron-induced retinal damage by determining lipid peroxidation levels and cell viability. To this end, entire isolated retinas were incubated in the presence of variable concentrations of $FeSO_4$ (25, 200 and 800 μM) for different periods of time (5 and 60 min). Controls were also assessed by replacing Fe^{2+} by an equal volume of water (vehicle). The generation of malondialdehyde, a marker of lipid peroxidation, was analyzed by measuring TBARS. As shown in Fig. 1A and B, TBARS generation was found to be increased in a Fe^{2+} concentration- and time-dependent manner. The increase in lipid peroxidation products could be immediately observed. After a 5 min exposure to the metal, TBARS increased by 0.6, 2.2 and 3.6 times with respect to controls at 25, 200 and 800 μM Fe^{2+}, respectively (Fig. 1A). Maximal malondialdehyde generation was observed after 60 min of Fe^{2+} exposure (Fig. 1B). Under these experimental conditions, TBARS levels were 1.8, 6.5, and 9 times higher than controls at 25, 200 and 800 μM Fe^{2+}, respectively.

Retinal cell viability was analyzed by measuring MTT reduction under the same above-mentioned experimental conditions. After 5 min of incubation with 25, 200 and 800 μM Fe^{2+} it showed no changes (Fig. 1C) while it was observed to be affected at 200 and 800 μM Fe^{2+} after 60 min of incubation (Fig. 1D).

3.2. MAPK activation and tyrosine phosphorylation are triggered during iron-induced retinal toxicity

Since MAPKs ERK1/2 and p38 are known to be activated by iron-induced oxidative stress in neuronal and non-neuronal tissues (Salvador and Oteiza, 2011; Uranga et al., 2009), we also investigated the possible activation of these MAPKs in retinas exposed to Fe^{2+}. Fig. 2A shows that Fe^{2+} exposure induced an increase in ERK1/2 phosphorylation after 60 min of incubation. ERK1/2 phosphorylation levels increased significantly at 25 μM Fe^{2+}, reaching maximum levels (160% increase) at 800 μM Fe^{2+}. An increase in p38 phosphorylation was only evident in the presence of 25 μM Fe^{2+} during the same incubation time period (Fig. 2B).

Tyrosine phosphorylation profile was also analyzed by using an anti-phosphotyrosine antibody (PY20) in retinas exposed to Fe^{2+} for 60 min. Iron-induced oxidative injury triggered a marked increase in the phosphorylation of tyrosines of several retinal proteins (Fig. 2C).

3.3. $cPLA_2$ and $iPLA_2$ activities are differentially regulated during iron-induced retinal toxicity

In order to characterize PLA_2 activities during iron-induced retinal toxicity, AA and palmitic acid (PAL) release was analyzed in total homogenate, mitochondrial, microsomal and cytosolic fractions

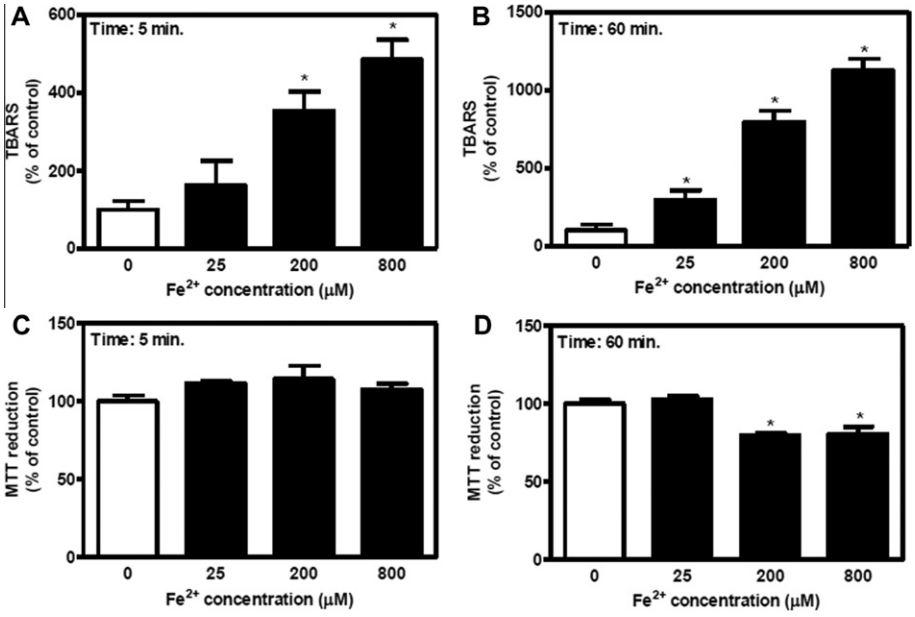

Fig. 1. Characterization of Fe^{2+}-induced damage in the retina. (A and B) Lipid peroxidation assay performed in homogenates of retinas exposed to 25, 200, and 800 μM Fe^{2+} for 5 min (A) and 60 min (B). (C and D) Measurement of MTT reduction after the same incubation times and the same iron concentrations. Results are shown as a percentage of control and represent the mean ± SD of at least three independent experiments. *Significantly different compared to the respective control group ($p < 0.05$, one-way ANOVA test followed by LSD test).

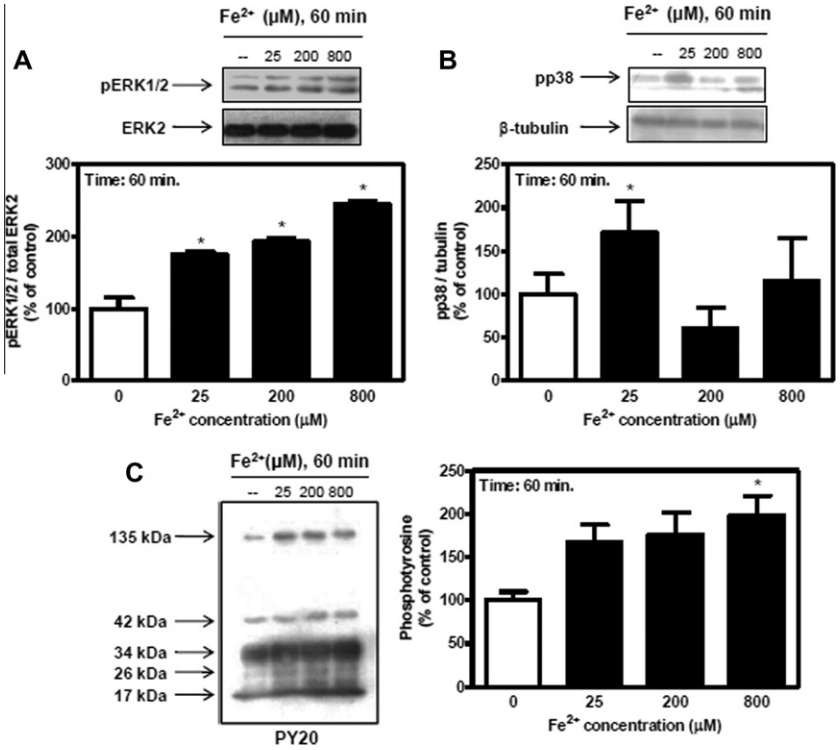

Fig. 2. Effect of Fe^{2+} exposure on MAPK and tyrosine phosphorylation. (A) Western blot analysis of ERK1/2 phosphorylation performed in homogenates of retinas (30 μg protein per lane) exposed to 25, 200, and 800 μM Fe^{2+} for 60 min. (B) p38 Phosphorylation assessed under the same experimental conditions as those described in (A). (C) Tyrosine phosphorylation pattern analyzed by Western blot under the same conditions as those described in (A and B). One representative Western blot image (for PY20) of three different experiments is shown. Bands of proteins were quantified using scanning densitometry, and phospho-ERK1/2 levels were normalized to ERK2 levels and phospho-p38 levels were normalized to β-tubulin levels. Results are shown as a percentage of the corresponding control conditions and represent the mean ± SD of at least three independent experiments. *Significantly different compared to the respective control group ($p < 0.05$, one-way ANOVA test followed by LSD test).

isolated after retinal iron exposure. $cPLA_2$ was assayed by measuring [^{14}C]AA release in a buffer containing calcium and using [^{14}C]PAPC as exogenous substrate. [^{14}C]AA release was barely affected in retinal homogenates and mitochondrial fraction after iron exposure with respect to controls (data not shown). The most striking changes in $cPLA_2$ activity were observed in microsomal and cytosolic fractions. After 5 and 60 min of Fe^{2+} exposure, a strong inhibition of microsomal $cPLA_2$ activity (by approximately 50%) and a slight increase in [^{14}C]AA release (20%) in the cytosol were observed (Fig. 3A and B). Under control conditions, there were no differences in the levels of [^{14}C]AA release. However, in the retinas exposed to iron, [^{14}C]AA levels in the cytosolic fraction were higher (by approximately 100–200%) than those released in the microsomal fractions (Fig. 3A and B).

[^{14}C]AA generation from PAPC could also be produced by the sequential action of phospholipase A_1 and lysophospholipase A_2. 2-Arachidonoyl-lysophosphatidylcholine (LPC) generated by phospholipase A_1 could be hydrolyzed by lysophospholipase A_2 yielding AA. Under our experimental conditions, LPC generation was barely detected both under control and experimental conditions (data not shown). In the presence of 2 mM PMSF (used as lysophospholipase A_2 inhibitor), there were no changes in the increase of [^{14}C]AA generation observed in the cytosolic fractions (data not shown). Based on these experiments, we can assume that the major pathway for [^{14}C]AA generation in retinas exposed to iron-induced oxidative stress is phospholipase A_2.

$iPLA_2$ activity was assayed in the presence of exogenous [^{14}C]DPPC as substrate in a buffer containing EDTA and ATP (Fig. 3C and D). [^{14}C]PAL release was inhibited in microsomal fractions with respect to controls, by 33%, 70% and 83% at 25 μM, 200 μM and 800 μM Fe^{2+}, respectively. In cytosolic fractions, [^{14}C]PAL release was higher than that observed in microsomes at all iron concentrations assayed. As it was observed for $cPLA_2$, iron-induced oxidative stress provoked an increase in [^{14}C]PAL release in cytosolic fractions with respect to microsomes after 5 min of incubation, at all iron concentrations assayed (Fig. 3C). After 60 min of iron exposure, a strong inhibition of [^{14}C]PAL liberation in microsomal fractions was also observed. However, during this incubation time period, no iron-induced differences in $iPLA_2$ activity between microsomal and cytosolic fractions were observed (Fig. 3D). It is important to note that $iPLA_2$ activity was one time higher after 5 min of Fe^{2+} exposure than that observed after 60 min of metal exposure at all iron concentrations assayed. Furthermore, as it was observed for $cPLA_2$, $iPLA_2$ activity showed no significant changes during iron-induced oxidative stress in retinal homogenates and mitochondrial fractions (data not shown).

3.4. $cPLA_2$ and $iPLA_2$ participate in the generation of lipid peroxides during iron-induced retinal toxicity

In order to characterize the role of PLA_2 in retinal oxidative damage, we further investigated the generation of lipid peroxidation products in the presence of PLA_2 isoform-specific inhibitors. To this end, retinas were preincubated with 50 μM ATK ($cPLA_2$ inhibitor) or 25 μM BEL ($iPLA_2$ inhibitor) and after iron exposure TBARS were determined. In the presence of ATK, there was a 50% decrease in TBARS generation at all iron concentrations assayed (Fig. 4A). In contrast, in the presence of BEL, TBARS formation was increased at 200 and 800 μM Fe^{2+} (Fig. 4B).

For the determination of the role of PLA_2 isoforms in retinal cell viability, MTT reduction was measured in the presence of the above-mentioned PLA_2 inhibitors. Neither ATK nor BEL could mod-

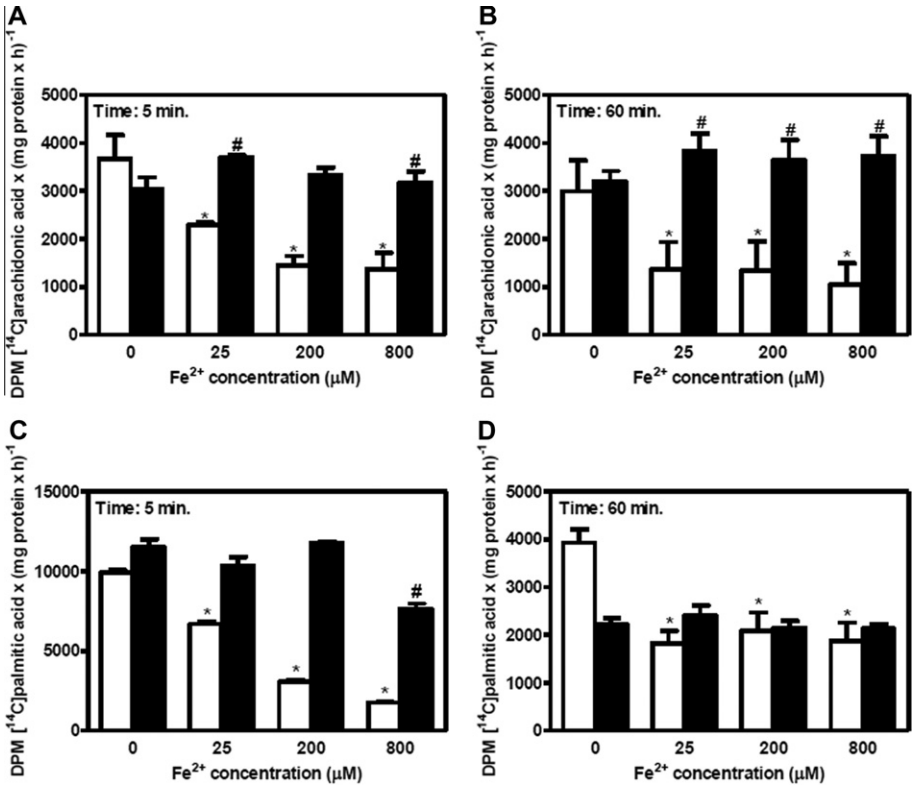

Fig. 3. Effect of Fe^{2+} exposure on microsomal and cytosolic PLA_2 activities. (A and B) $cPLA_2$ activity evaluated in microsomal (□) and cytosolic (■) fractions obtained from retinas exposed to 25, 200, and 800 μM Fe^{2+} for 5 min (A) and 60 min (B). Results are expressed as DPM [^{14}C]arachidonic acid × (mg protein × h)$^{-1}$ and represent the mean ± SD of at least three independent experiments. (C and D) $iPLA_2$ activity determined in the same retinal subcellular fractions and conditions as those used for $cPLA_2$ after 5 min (C) and 60 min (D) of Fe^{2+} exposure. Results are expressed as DPM [^{14}C]palmitic acid × (mg protein × h)$^{-1}$ and represent the mean ± SD of at least three independent experiments. *Significantly different compared to the respective control group for microsomal samples ($p < 0.05$, one-way ANOVA test followed by LSD test). #Significantly different compared to the respective control group for cytosolic samples ($p < 0.05$, one-way ANOVA test, followed by LSD test).

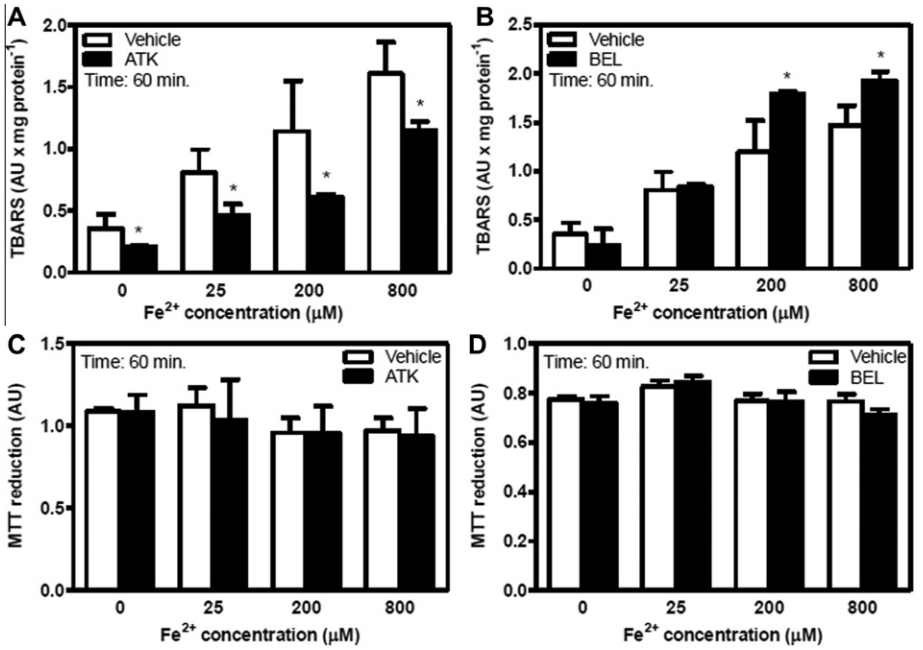

Fig. 4. Effect of PLA_2 inhibition on Fe^{2+}-induced damage in the retina. (A and B) Lipid peroxidation assessed in homogenates obtained from retinas exposed for 60 min to 25, 200, and 800 μM Fe^{2+} in the presence or absence of two PLA_2 inhibitors: ATK (50 μM, A) and BEL (25 μM, B). (C and D) MTT decrease analyzed under the same conditions as those described for lipid peroxidation assay. PLA_2 inhibitors ATK (C) and BEL (D) were used in the same concentrations as specified in (A). Results are expressed as a percentage of control and represent the mean ± SD of three independent experiments. *Significantly different compared to the respective control group ($p < 0.05$, one-way ANOVA test, followed by LSD test).

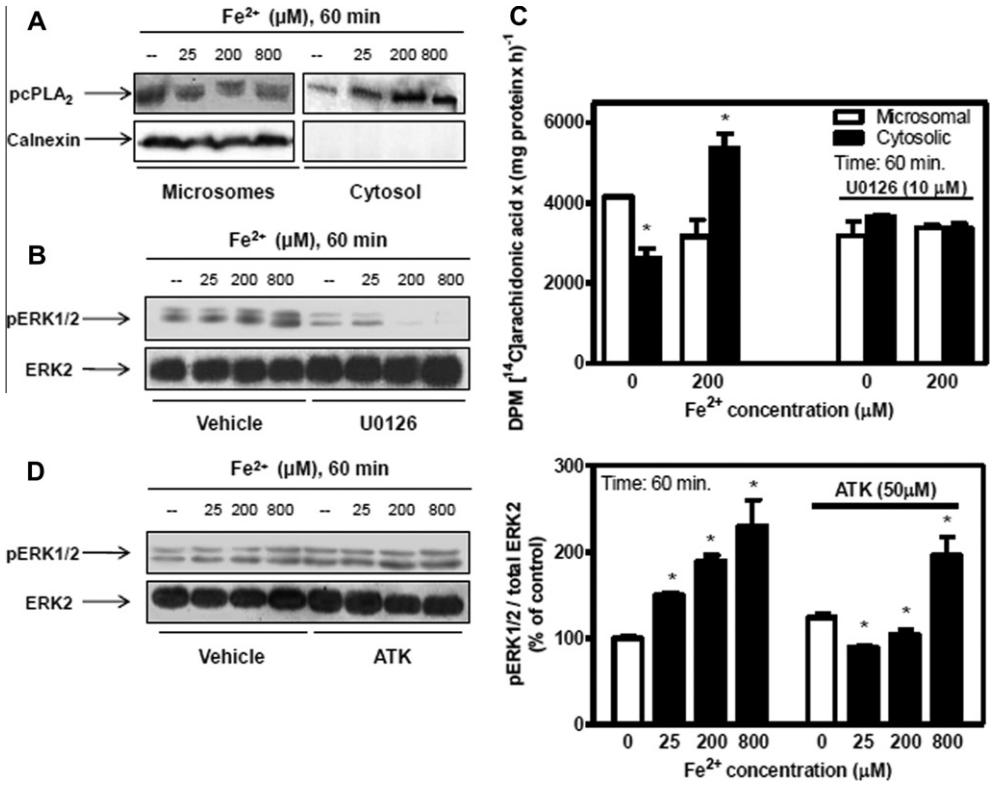

Fig. 5. Crosstalk between PLA_2 and ERK1/2 under Fe^{2+}-induced oxidative stress. (A) Western blot analysis of $cPLA_2$ phosphorylation in microsomal and cytosolic fractions obtained from retinas (30 μg protein per lane) exposed to 25, 200, and 800 μM Fe^{2+} for 60 min. Calnexin was used as loading control. One representative Western blot image of three different experiments is shown. Western blot analysis of ERK1/2 phosphorylation in homogenates of retinas (30 μg protein per lane) preincubated with either U0126 (10 μM, B) or ATK (50 μM, D) and then exposed to 25, 200, and 800 μM Fe^{2+} for 60 min. One representative Western blot image of three different experiments is shown. Bands of proteins were quantified using scanning densitometry, and phospho-ERK1/2 levels were normalized to total ERK2 levels. Results are shown as a percentage of the corresponding control condition and represent the mean ± SD of at least three independent experiments. *Significantly different compared to the respective control group ($p < 0.05$, one-way ANOVA test followed by LSD test). (C) $cPLA_2$ activity analyzed in microsomal and cytosolic fractions obtained from retinas preincubated with 10 μM U0126 or the vehicle, and then exposed to 200 μM Fe^{2+} for 60 min and in the presence or absence of U0126. Results are expressed as DPM [^{14}C]arachidonic acid × (mg protein × h)$^{-1}$ and represent the mean ± SD of at least three independent experiments. *Significantly different compared to the respective control group ($p < 0.05$, one-way ANOVA test, followed by LSD test).

ify retinal cell viability under all experimental conditions assayed (Fig. 4C and D).

3.5. Cross-talk between $cPLA_2$ and ERK1/2 during iron-induced retinal toxicity

One of the most common mechanisms of $cPLA_2$ activation is its phosphorylation by ERK1/2 (Chakraborti, 2003; Ghosh et al., 2006; Leslie, 1997; Mariggio et al., 2006; Nicotra et al., 2005; Zhu et al., 2001). $cPLA_2$ phosphorylation in Ser 505 was inhibited in the microsomal fractions from retinas exposed to iron. In contrast, $cPLA_2$ phosphorylation was increased in the cytosolic fractions obtained from retinas exposed to iron (Fig. 5A). In order to establish a correlation between the activation of ERK1/2 and the differential release of AA during iron-induced oxidative stress, $cPLA_2$ activity was analyzed in retinas preincubated with MAPK inhibitor U0126. In the presence of U0126, ERK1/2 phosphorylation was inhibited at all iron concentrations assayed (Fig. 5B). Under these experimental conditions, the inhibition of AA release in microsomal fractions and the increase of AA release in cytosolic fractions provoked by iron exposure (200 μM) were completely abolished (Fig. 5C).

We also checked the state of ERK1/2 phosphorylation in the presence of $cPLA_2$ inhibitor. ATK was found to inhibit the increase in ERK1/2 phosphorylation previously observed at 25 and 200 μM Fe^{2+} (Fig. 5D). At 800 μM Fe^{2+}, ERK1/2 activation underwent no changes in the presence of ATK.

3.6. COX-2 expression and activity increase during iron-induced retinal toxicity

COX-2 and $cPLA_2$ are involved in eicosanoid production and they also seem to participate in several pathological processes such as the progression of several types of cancer and oxidative stress events (Linkous et al., 2010). We therefore further studied if iron-induced retinal toxicity could affect COX-2 expression. COX-2 association with microsomal membranes augmented as a function of iron concentration, this increase being 80%, 170% and 210% higher than that in controls (Fig. 6A). The generation of PGF_2 and PGE_2, the main products of COX-2 activity, was increased in retinas exposed to 25 μM Fe^{2+} (Fig. 6B).

4. Discussion

Retinal damage is a major concern in relation to a number of ocular diseases leading to blindness. AMD, one of these devastating conditions, is characterized by the deterioration of the macula which severely impairs central vision. Based on observations showing iron overload in retinas of AMD patients compared to healthy subjects, excessive retinal iron content and the resulting oxidative stress condition have been proposed to contribute to this pathology (Dunaief, 2006). A poorly studied issue is the connection between iron-induced oxidative stress, retinal degeneration and the associated signaling events. Further studies in this direction

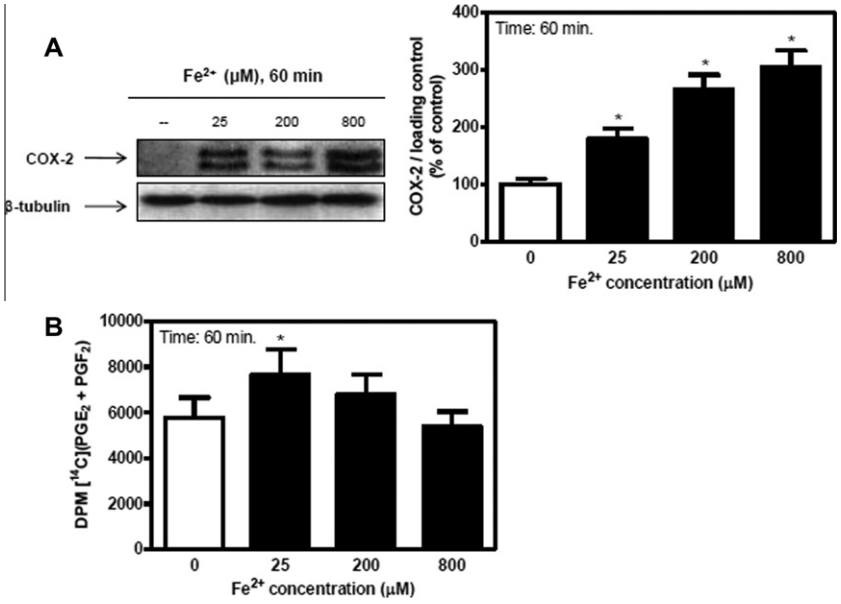

Fig. 6. COX-2 microsomal expression and prostaglandin synthesis under Fe^{2+}-induced oxidative stress. (A) COX-2 expression evaluated in microsomal fractions of retinas (30 μg protein per lane) exposed to 25, 200, and 800 μM Fe^{2+} for 60 min. COX-2 levels were normalized to β-tubulin levels and expressed as a percentage of the control condition and represent the mean ± SD of at least three independent experiments. (B) COX-2 activity was analyzed in microsomal fractions obtained from retinas exposed to 25, 200, and 800 μM Fe^{2+} for 60 min. Results are expressed as DPM [^{14}C](PGE_2 + PGF_2) and represent the mean ± SD of at least three independent experiments. *Significantly different compared to the respective control group ($p < 0.05$, one-way ANOVA test, followed by LSD test).

will therefore uncover clues to AMD pathogenesis and lead to new preventive or therapeutic strategies.

The main purpose of this work was to study the role of different PLA_2 isoforms in bovine retinas exposed to increasing iron concentrations as an experimental model of AMD. PLA_2 generates AA, docosahexaenoic acid and lysophospholipids from neuronal membrane phospholipids (Kolko et al., 2009). All these products were named bioactive lipids because they have a variety of physiological effects by themselves and because they are also substrates for the synthesis of more potent lipid mediators, such as eicosanoids, platelet activating factor, and 4-hydroxynonenal (4-HNE). The lipid peroxidation product 4-HNE is one of the most cytotoxic metabolites and is associated with the apoptotic type of neuronal cell death. $cPLA_2$ has particularly been involved in the generation of ROS through AA release in cerebral ischemia events (Adibhatla and Hatcher, 2010). On the other hand, after the discovery of neuroprotectins, PLA_2 was found to be implicated in signaling mechanisms involved in neuroprotection (Bazan, 2009).

As stated earlier, oxidative stress has been found to be involved in the pathogenesis of AMD. Increased iron concentrations, which generate highly reactive hydroxyl radicals via the Fenton reaction, may induce oxidative stress in the macula and lead to AMD. Increased iron concentrations in AMD-affected eyes are formed, in part, of a chelatable iron pool, this being the reason for incubating retinas with increasing $FeSO_4$ concentrations (a form of chelatable iron) as an AMD model (Blasiak et al., 2011). The choice of 25, 200 and 800 μM Fe^{2+} concentrations was based on the results shown in Fig. 1A–D, which are indicative of increased oxidative retinal damage and loss of cell viability as a function of iron concentration. The retinas exposed to Fe^{2+} evidenced an increase in lipid peroxidation even after short incubation periods. $FeSO_4$ at its maximal concentration (800 μM) provoked TBARS generation to be 5 and 10 times higher after an incubation period of 5 and 60 min, respectively. Furthermore, in spite of the strong rise of lipid peroxidation products, there were no changes in cellular viability after 5 min of incubation at all iron concentrations assayed. A small decrease (20% with respect to controls) in mitochondrial function was only observed at 200 and 800 μM Fe^{2+} after 60 min of incubation. These results were in accordance with the slight decrease (lower than 20%) in the retinal radical scavenging capacity only observed at 200 and 800 μM Fe^{2+} and after 60 min of incubation (data not shown). Our results confirm the vast resistance of the retina to oxidative stress and also support the use of antioxidant therapies for preventing oxidative stress-induced retinal degeneration (Stahl and Sies, 2005; Usui et al., 2009).

In our study, it was also possible to observe that iron-induced retinal damage caused a differential profile in AA release in microsomal and cytosolic fractions. AA release was measured in a buffer containing calcium and under conditions that promote $cPLA_2$ activity. Whereas a strong inhibition of AA release was detected in the microsomal fractions at all iron concentrations assayed, an increase in cytosolic AA production was observed. Moreover, when comparing microsomes vs. cytosols, it was observed that AA release was higher in the soluble fraction of the retinas exposed to iron. A rapid metabolization of AA could be the reason for the decreased AA detection observed in microsomes from the retinas exposed to iron. To gain a better insight into the mechanism intervening in AA metabolization, we next examined the expression of COX-2 in microsomal fractions. COX, which exists in two major isoforms, COX-1 and -2, catalyzes the second step in the conversion of AA to prostaglandins (Fang et al., 2007). In most tissues, COX-1 is thought to be responsible for the production of prostaglandins associated with homeostatic functions whereas COX-2 is usually induced in several cell types in response to inflammatory stimuli (Kaufmann et al., 1997). In our experimental system, COX-2 association with microsomal membranes increased as a function of iron concentration and, consequently, with lipid peroxidation. The association of COX-2 with microsomes is indicative of prostaglandin generation as one of the main products derived from $cPLA_2$ activation. These results argue in favor of a rapid metabolization of AA in microsomal membranes catalyzed by the presence of COX-2 during iron-induced retinal damage. The increase of both AA release and the phosphorylated form of $cPLA_2$ in cytosolic fractions seems to be indicative of a compensatory mechanism for

excluding activated $cPLA_2$ from microsomal membranes during iron-induced retinal toxicity.

Previous research has demonstrated that $iPLA_2$-VIA is involved in the regulation of retinal pigment epithelium phagocytosis of photoreceptor outer segments and that it may be also involved in the regulation of photoreceptor cell renewal (Kolko et al., 2007). $iPLA_2$ activity in the proposed model was measured by quantification of PAL release. $iPLA_2$ activity showed a similar profile than that observed for $cPLA_2$ after a short time of oxidative injury (Kolko et al., 2009). After 60 min of iron-induced retinal damage, PAL release showed no differences between microsomal and cytosolic fractions. However, it is important to note that after 5 min of iron exposure, $iPLA_2$ activity was higher than after 60 min of incubation with the metal. These results argue in favor of an active participation of $iPLA_2$ activity, particularly at short incubation time periods.

ATK and BEL were used in order to determine the role of $cPLA_2$ and $iPLA_2$ in iron-induced retinal lipid peroxidation. ATK was observed to be able to prevent iron-induced lipid peroxidation from increasing whereas BEL generated the opposite effect. These results are indicative of a differential participation of these isoforms in the lipid peroxidation process. A similar role for $cPLA_2$ has been reported in relation to cerebral ischemia and many other brain pathologies (Adibhatla and Hatcher, 2010; Kishimoto et al., 2010). The inhibition of $cPLA_2$ by Ginkgo biloba extract has been shown to provide protection against oxidative stress-induced neuronal death (Zhao et al., 2011). Results obtained for $iPLA_2$ indicate a potentially protective role against lipid peroxidation. This could be in accordance with the participation of $iPLA_2$ in phospholipid remodeling process (Balsinde et al., 2006). Our results show that even though PLA_2 isoforms are involved in the lipid peroxidation process, their participation does not affect cellular viability.

ERK1/2 activation has been reported to be involved both in neuronal survival and cellular death. One of the multiple physiological targets of ERK1/2 is $cPLA_2$. This PLA_2 isoform is activated when serines 505 and 727 are ERK1/2. We demonstrate here that iron-induced retinal oxidative stress activates ERK1/2 and that the localization of AA release between cytosolic and microsomal compartments is a mechanism regulated by ERK1/2. It could also be observed that iron-induced oxidative stress increases AA release in the cytosolic fraction and $cPLA_2$ inhibition by ATK attenuated ERK1/2 activation at 25 and 200 μM Fe^{2+}, thus highlighting the importance of PLA_2 as a mediator of MAPK signaling during iron-induced retinal degeneration. Similar results were observed in cyclic stretching of rabbit proximal tubular cells (Alexander et al., 2004). These findings support the hypothesis of a bidirectional regulation between $cPLA_2$ and ERK1/2 during iron-induced retinal oxidative stress, which, in turn, suggests a direct relationship between $cPLA_2$ activity, lipid peroxidation and ERK1/2 activation.

The implications of $cPLA_2$ participation during iron-induced RD and the way in which this enzyme could be used as a therapeutic target against iron overload-related diseases have not yet been fully elucidated. Nonetheless, our findings about retinal acute exposure to iron could contribute to the understanding of the molecular mechanisms underlying more chronic processes triggered by iron accumulation which could be involved in the pathogenesis of AMD.

Funding

This work was supported by Grants from the Universidad Nacional del Sur, the Consejo Nacional de Investigaciones Científicas y Técnicas [Grant No. PIP 11220090100687] (CONICET), the Fundación Florencio Fiorini and the Agencia Nacional de Promoción Científica y Tecnológica [Grant No. PICT-2010-0936] (ANPCYT).

Acknowledgements

R.M.U., M.V.M., N.M.G. and G.A.S. are research members of the CONICET. G.R.D. is a research fellow of the CONICET. We thank Frigorífico Villa Olga and Frigorífico Viñuela, especially Dr. Francisco Príncipe, Dr. Daniel Boero and Mr. José Belmar for kindly providing bovine eyes. We specially thank Dr. Beatriz Caputto for kindly providing the anti-calnexin antibody.

References

Adibhatla, R.M., Hatcher, J.F., 2010. Lipid oxidation and peroxidation in CNS health and disease: from molecular mechanisms to therapeutic opportunities. Antioxid. Redox. Signal. 1, 125–169.
Alexander, L.D., Alagarsamy, S., Douglas, J.G., 2004. Cyclic stretch-induced cPLA2 mediates ERK 1/2 signaling in rabbit proximal tubule cells. Kidney Int. 2, 551–563.
Balsinde, J., Perez, R., Balboa, M.A., 2006. Calcium-independent phospholipase A2 and apoptosis. Biochim. Biophys. Acta 11, 1344–1350.
Bazan, N.G., 2009. Neuroprotectin D1-mediated anti-inflammatory and survival signaling in stroke, retinal degenerations, and Alzheimer's disease. J. Lipid Res., S400–S405.
Blasiak, J., Szaflik, J., Szaflik, J.P., 2011. Implications of altered iron homeostasis for age-related macular degeneration. Front. Biosci., 1551–1559.
Burke, J.E., Dennis, E.A., 2009a. Phospholipase A2 biochemistry. Cardiovasc. Drugs Ther. 1, 49–59.
Burke, J.E., Dennis, E.A., 2009b. Phospholipase A2 structure/function, mechanism, and signaling. J. Lipid Res., S237–S242.
Chakraborti, S., 2003. Phospholipase A(2) isoforms: a perspective. Cell Signal. 7, 637–665.
Dunaief, J.L., 2006. Iron induced oxidative damage as a potential factor in age-related macular degeneration: the Cogan lecture. Invest. Ophthalmol. Vis. Sci. 11, 4660–4664.
Dunaief, J.L., Richa, C., Franks, E.P., Schultze, R.L., Aleman, T.S., Schenck, J.F., Zimmerman, E.A., Brooks, D.G., 2005. Macular degeneration in a patient with aceruloplasminemia, a disease associated with retinal iron overload. Ophthalmology 6, 1062–1065.
Fang, I.M., Yang, C.H., Yang, C.M., Chen, M.S., 2007. Linoleic acid-induced expression of inducible nitric oxide synthase and cyclooxygenase II via p42/44 mitogen-activated protein kinase and nuclear factor-kappaB pathway in retinal pigment epithelial cells. Exp. Eye Res. 5, 667–677.
Farooqui, A.A., Ong, W.Y., Horrocks, L.A., 2006. Inhibitors of brain phospholipase A2 activity: their neuropharmacological effects and therapeutic importance for the treatment of neurologic disorders. Pharmacol. Rev. 3, 591–620.
Feder, J.N., Gnirke, A., Thomas, W., Tsuchihashi, Z., Ruddy, D.A., Basava, A., Dormishian, F., Domingo Jr., R., Ellis, M.C., Fullan, A., Hinton, L.M., Jones, N.L., Kimmel, B.E., Kronmal, G.S., Lauer, P., Lee, V.K., Loeb, D.B., Mapa, F.A., McClelland, E., Meyer, N.C., Mintier, G.A., Moeller, N., Moore, T., Morikang, E., Prass, C.E., Quintana, L., Starnes, S.M., Schatzman, R.C., Brunke, K.J., Drayna, D.T., Risch, N.J., Bacon, B.R., Wolff, R.K., 1996. A novel MHC class I-like gene is mutated in patients with hereditary haemochromatosis. Nat. Genet. 4, 399–408.
Feder, J.N., Penny, D.M., Irrinki, A., Lee, V.K., Lebron, J.A., Watson, N., Tsuchihashi, Z., Sigal, E., Bjorkman, P.J., Schatzman, R.C., 1998. The hemochromatosis gene product complexes with the transferrin receptor and lowers its affinity for ligand binding. Proc. Natl. Acad. Sci. USA 4, 1472–1477.
Folch, J., Lees, M., Sloane Stanley, G.H., 1957. A simple method for the isolation and purification of total lipids from animal tissues. J. Biol. Chem. 1, 497–509.
Franchi, A., Di, G.G., Farina, M., de los Santos, A.R., Marti, M.L., Gimeno, M.A., 2000. Differential action of non-steroidal antiinflammatory drugs on human gallbladder cyclooxygenase and lipoxygenase. Medicina (B Aires) 5 (Pt 1), 580–586.
Garcia-Castineiras, S., 2010. Iron, the retina and the lens: a focused review. Exp. Eye Res. 6, 664–678.
Ghosh, M., Tucker, D.E., Burchett, S.A., Leslie, C.C., 2006. Properties of the Group IV phospholipase A2 family. Prog. Lipid Res. 6, 487–510.
Hadziahmetovic, M., Dentchev, T., Song, Y., Haddad, N., He, X., Hahn, P., Pratico, D., Wen, R., Harris, Z.L., Lambris, J.D., Beard, J., Dunaief, J.L., 2008. Ceruloplasmin/hephaestin knockout mice model morphologic and molecular features of AMD. Invest. Ophthalmol. Vis. Sci. 6, 2728–2736.
Hahn, P., Qian, Y., Dentchev, T., Chen, L., Beard, J., Harris, Z.L., Dunaief, J.L., 2004. Disruption of ceruloplasmin and hephaestin in mice causes retinal iron overload and retinal degeneration with features of age-related macular degeneration. Proc. Natl. Acad. Sci. USA 38, 13850–13855.
He, X., Hahn, P., Iacovelli, J., Wong, R., King, C., Bhisitkul, R., Massaro-Giordano, M., Dunaief, J.L., 2007. Iron homeostasis and toxicity in retinal degeneration. Prog. Retin. Eye Res. 6, 649–673.
Kashiwagi, T., Meyer-Rochow, V.B., Nishimura, K., Eguchi, E., 2000. Light activation of phospholipase A2 in the photoreceptor of the crayfish (*Procambarus clarkii*). Acta Neurobiol. Exp. (Wars) 1, 9–16.
Kaufmann, W.E., Andreasson, K.I., Isakson, P.C., Worley, P.F., 1997. Cyclooxygenases and the central nervous system. Prostaglandins 3, 601–624.
Kishimoto, K., Li, R.C., Zhang, J., Klaus, J.A., Kibler, K.K., Dore, S., Koehler, R.C., Sapirstein, A., 2010. Cytosolic phospholipase A2 alpha amplifies early

cyclooxygenase-2 expression, oxidative stress and MAP kinase phosphorylation after cerebral ischemia in mice. J. Neuroinflammation, 42.
Kolko, M., Wang, J., Zhan, C., Poulsen, K.A., Prause, J.U., Nissen, M.H., Heegaard, S., Bazan, N.G., 2007. Identification of intracellular phospholipases A2 in the human eye: involvement in phagocytosis of photoreceptor outer segments. Invest. Ophthalmol. Vis. Sci. 3, 1401–1409.
Kolko, M., Kiilgaard, J.F., Wang, J., Poulsen, K.A., Andreasen, J.R., Ia, C.M., Nissen, M.H., Heegaard, S., Bazan, N.G., Prause, J.U., 2009. Calcium-independent phospholipase A2 regulates retinal pigment epithelium proliferation and may be important in the pathogenesis of retinal diseases. Exp. Eye Res. 3, 383–391.
Laemmli, U.K., 1970. Cleavage of structural proteins during the assembly of the head of bacteriophage T4. Nature 5259, 680–685.
Leslie, C.C., 1997. Properties and regulation of cytosolic phospholipase A2. J. Biol. Chem. 27, 16709–16712.
Linkous, A.G., Yazlovitskaya, E.M., Hallahan, D.E., 2010. Cytosolic phospholipase A2 and lysophospholipids in tumor angiogenesis. J. Natl. Cancer Inst. 18, 1398–1412.
Lowry, O.H., Rosebrough, N.J., Farr, A.L., Randall, R.J., 1951. Protein measurement with the Folin phenol reagent. J. Biol. Chem. 1, 265–275.
Lukinova, N., Iacovelli, J., Dentchev, T., Wolkow, N., Hunter, A., Amado, D., Ying, G.S., Sparrow, J.R., Dunaief, J.L., 2009. Iron chelation protects the retinal pigment epithelial cell line ARPE-19 against cell death triggered by diverse stimuli. Invest. Ophthalmol. Vis. Sci. 3, 1440–1447.
Mariggio, S., Bavec, A., Natale, E., Zizza, P., Salmona, M., Corda, D., Di, G.M., 2006. Galpha13 mediates activation of the cytosolic phospholipase A2alpha through fine regulation of ERK phosphorylation. Cell Signal. 12, 2200–2208.
Mateos, M.V., Uranga, R.M., Salvador, G.A., Giusto, N.M., 2008. Activation of phosphatidylcholine signalling during oxidative stress in synaptic endings. Neurochem. Int. 6–8, 199–206.
Morgan, N.V., Westaway, S.K., Morton, J.E., Gregory, A., Gissen, P., Sonek, S., Cangul, H., Coryell, J., Canham, N., Nardocci, N., Zorzi, G., Pasha, S., Rodriguez, D., Desguerre, I., Mubaidin, A., Bertini, E., Trembath, R.C., Simonati, A., Schanen, C., Johnson, C.A., Levinson, B., Woods, C.G., Wilmot, B., Kramer, P., Gitschier, J., Maher, E.R., Hayflick, S.J., 2006. PLA2G6, encoding a phospholipase A2, is mutated in neurodegenerative disorders with high brain iron. Nat. Genet. 7, 752–754.
Moses, G.S., Jensen, M.D., Lue, L.F., Walker, D.G., Sun, A.Y., Simonyi, A., Sun, G.Y., 2006. Secretory PLA2-IIA: a new inflammatory factor for Alzheimer's disease. J. Neuroinflammation, 28.
Nicotra, A., Lupo, G., Giurdanella, G., Anfuso, C.D., Ragusa, N., Tirolo, C., Marchetti, B., Alberghina, M., 2005. MAPKs mediate the activation of cytosolic phospholipase A2 by amyloid beta (25–35) peptide in bovine retina pericytes. Biochim. Biophys. Acta 2–3, 172–186.
Pete, M.J., Wu, D.W., Exton, J.H., 1996. Subcellular fractions of bovine brain degrade phosphatidylcholine by sequential deacylation of the sn-1 and sn-2 positions. Biochim. Biophys. Acta 3, 325–332.
Salvador, G.A., Giusto, N.M., 2006. Phospholipase D from photoreceptor rod outer segments is a downstream effector of RhoA: evidence of a light-dependent mechanism. Exp. Eye Res. 1, 202–211.
Salvador, G.A., Oteiza, P.I., 2011. Iron overload triggers redox-sensitive signals in human IMR-32 neuroblastoma cells. Neurotoxicology 1, 75–82.
Stahl, W., Sies, H., 2005. Bioactivity and protective effects of natural carotenoids. Biochim. Biophys. Acta 2, 101–107.
Sun, G.Y., Horrocks, L.A., Farooqui, A.A., 2007. The roles of NADPH oxidase and phospholipases A2 in oxidative and inflammatory responses in neurodegenerative diseases. J. Neurochem. 1, 1–16.
Sun, G.Y., Shelat, P.B., Jensen, M.B., He, Y., Sun, A.Y., Simonyi, A., 2010. Phospholipases A2 and inflammatory responses in the central nervous system. Neuromolecular. Med. 2, 133–148.
Svensson, C.I., Lucas, K.K., Hua, X.Y., Powell, H.C., Dennis, E.A., Yaksh, T.L., 2005. Spinal phospholipase A2 in inflammatory hyperalgesia: role of the small, secretory phospholipase A2. Neuroscience 2, 543–553.
Tanito, M., Kaidzu, S., Ohira, A., Anderson, R.E., 2008. Topography of retinal damage in light-exposed albino rats. Exp. Eye Res. 3, 292–295.
Uranga, R.M., Mateos, M.V., Giusto, N.M., Salvador, G.A., 2007. Activation of phosphoinositide-3 kinase/Akt pathway by $FeSO_4$ in rat cerebral cortex synaptic endings. J. Neurosci. Res. 13, 2924–2932.
Uranga, R.M., Giusto, N.M., Salvador, G.A., 2009. Iron-induced oxidative injury differentially regulates PI3K/Akt/GSK3beta pathway in synaptic endings from adult and aged rats. Toxicol. Sci. 2, 331–344.
Usui, S., Komeima, K., Lee, S.Y., Jo, Y.J., Ueno, S., Rogers, B.S., Wu, Z., Shen, J., Lu, L., Oveson, B.C., Rabinovitch, P.S., Campochiaro, P.A., 2009. Increased expression of catalase and superoxide dismutase 2 reduces cone cell death in retinitis pigmentosa. Mol. Ther. 5, 778–786.
Wang, J., Kolko, M., 2010. Phospholipases A2 in ocular homeostasis and diseases. Biochimie 6, 611–619.
Wong, R.W., Richa, D.C., Hahn, P., Green, W.R., Dunaief, J.L., 2007. Iron toxicity as a potential factor in AMD. Retina 8, 997–1003.
Yagami, T., Ueda, K., Asakura, K., Hata, S., Kuroda, T., Sakaeda, T., Takasu, N., Tanaka, K., Gemba, T., Hori, Y., 2002. Human group IIA secretory phospholipase A2 induces neuronal cell death via apoptosis. Mol. Pharmacol. 1, 114–126.
Yang, L.P., Wu, L.M., Guo, X.J., Li, Y., Tso, M.O., 2008. Endoplasmic reticulum stress is activated in light-induced retinal degeneration. J. Neurosci. Res. 4, 910–919.
Zhao, Z., Liu, N., Huang, J., Lu, P.H., Xu, X.M., 2011. Inhibition of cPLA2 activation by *Ginkgo biloba* extract protects spinal cord neurons from glutamate excitotoxicity and oxidative stress-induced cell death. J. Neurochem. 6, 1057–1065.
Zhu, X., Sano, H., Kim, K.P., Sano, A., Boetticher, E., Munoz, N.M., Cho, W., Leff, A.R., 2001. Role of mitogen-activated protein kinase-mediated cytosolic phospholipase A2 activation in arachidonic acid metabolism in human eosinophils. J. Immunol. 1, 461–468.